Cement & Concrete Composites 31 (2009) 232–243

Contents lists available at ScienceDirect

Cement & Concrete Composites

journal homepage: www.elsevier.com/locate/cemconcomp

Fracture and fatigue of natural fiber-reinforced cementitious composites

H. Savastano Jr. [a,*], S.F. Santos [a], M. Radonjic [b], W.O. Soboyejo [b]

[a] Rural Construction Group, Faculty of Animal Science and Food Engineering, University of São Paulo, Caixa Postal 23, 13635-900 Pirassununga, SP, Brazil
[b] Princeton Institute of Science and Technology of Materials, and The Department of Mechanical and Aerospace Engineering, Princeton University, D404 E.-Quad., Olden Street, Princeton, NJ 08544, USA

ARTICLE INFO

Article history:
Received 21 November 2007
Received in revised form 31 January 2009
Accepted 3 February 2009
Available online 12 February 2009

Keywords:
Natural fibers
Cementitious matrices
Resistance-curve behavior
Fatigue crack growth
Crack-bridging

ABSTRACT

This paper presents the results of an experimental study of resistance-curve behavior and fatigue crack growth in cementitious matrices reinforced with eco-friendly natural fibers obtained from agricultural by-products. The composites include: blast furnace slag cement reinforced with pulped fibers of sisal, banana and bleached eucalyptus pulp, and ordinary Portland cement composites reinforced with bleached eucalyptus pulp. Fracture resistance (*R*-curve) and fatigue crack growth behavior were studied using single-edge notched bend specimens. The observed stable crack growth behavior was then related to crack/microstructure interactions that were elucidated via scanning electron microscopy (SEM) and energy dispersive X-ray spectroscopy (EDS). Fracture mechanics models were used to quantify the observed crack-tip shielding due to crack-bridging. The implications of the results are also discussed for the design of natural fiber-reinforced composite materials for affordable housing.

1. Introduction

In recent years, there have been considerable efforts to develop natural fiber-reinforced cementitious composites for affordable infrastructure [1]. However, the long term durability of natural fiber-reinforced composites may be limited due to their elevated permeability and lack of resistance to crack growth [2]. The vegetable fibers themselves can deteriorate due to the attack of the alkaline environment generated by the cement-based matrix or suffer mineralization associated to the internal deposition of hydration products in the fiber pores, what is another point of concern to overcome as a limitation in the use of vegetable fibers [1,2]. Additionally, to advance in the use of vegetable fibers it is essential to further study the crack/microstructure interactions and the interfacial transition zone between fibers and cementitious matrix. These are not properties that can be optimized simply by the design alterations for improved strength. Instead, a more balanced approach is needed for the optimization of strength, fracture toughness/resistance-curve behavior, fatigue resistance and reduced permeability.

Prior work on natural fiber-reinforced composites has focused largely on refined processes that can not be adopted easily in developing countries due to their relatively high costs [3]. There is, therefore, a need for simple, scalable processes that can be used readily by people in developing countries to make affordable building materials for eco-friendly infrastructure. Furthermore, since these buildings are likely to encounter a range of static overload and cyclic loading due to possible wind or earthquake loading, it is important to use rigorous fracture mechanics approaches to understand the conditions that lead to crack initiation and growth in natural fiber-reinforced composites subjected to monotonic or cyclic loading.

This paper presents the results of a combined experimental and theoretical study of *R*-curve behavior and fatigue crack growth in vegetable fiber-reinforced cementitious composites. The paper examines the effects of fiber reinforcement in composites, based on ground blast furnace slag (BFS) or ordinary Portland cement (OPC) with the replacement of about 66% of ground BFS, with commercial cellulose pulps of sisal, banana and eucalyptus. The performance of the cementitious composites reinforced with these vegetable fibers was evaluated after up to 2 years of aging in a laboratory environment. The single-edge notched bend specimens (SENB) were used in the present work. The measured resistance-curves are compared with predictions from theoretical fracture mechanics models [4–6]. The fatigue crack growth behavior is also elucidated with the crack/microstructure interactions that give rise to stable fatigue crack growth. Finally, the implications of the results are discussed for the design of affordable housing from natural fiber-reinforced composites.

2. Background

2.1. Physical and mechanical characterization of composites

In prior work, Savastano et al. [6–9] have analyzed the mechanical performance of the cement-based composites blended with ground blast furnace slag (BFS) and reinforced with eucalyptus,

* Corresponding author. Tel.: +55 19 35654200; fax: +55 19 35611689.
E-mail address: holmersj@usp.br (H. Savastano Jr.).

0958-9465/$ - see front matter © 2009 Elsevier Ltd. All rights reserved.
doi:10.1016/j.cemconcomp.2009.02.006

banana or sisal pulps. The sisal (*Agave sisalana*) and the banana (*Musa cavendishii*) crop wastes were subjected to chemo-thermo-mechanical pulping (CTMP) and Kraft methods, as suggested by Higgins [10].

Cement composite plates reinforced with 8 wt% of Kraft pulp (content based in the solid raw material) were prepared in the laboratory, using a slurry vacuum de-watering technique. A three-point bend configuration was applied in the determination of the modulus of rupture (MOR), modulus of elasticity (MOE) and toughness. Toughness was calculated by integration of the load–deflection curve to the point corresponding to a reduction in load carrying capacity to 50% of the maximum observed. The properties of cementitious composites at 28 days are presented in Table 1.

Non-aged composites had flexural strengths in excess of 16 MPa, representing ~100% improvement over a plain BFS matrix with corresponding design. As shown by Savastano et al. [11], 2 years of external exposure to tropical or temperate weather resulted in a considerable reduction in flexural strength. The modulus of rupture of the composite decreased from 18 MPa to about 5 MPa in the case of the 8 wt% sisal chemi-thermo-mechanical pulp (CTMP) formulation exposed to the tropical climate in Pirassununga, latitude 21°59′46", South, and longitude 47°25′33", West, altitude 627 m, state of São Paulo, Brazil.

The loss in mechanical strength of composites, subjected to either natural weathering or aging in a controlled environment, was attributed to the degradation of the vegetable fibers and of the cementitious matrix. The phenomenon of petrifaction can take place through the migration of hydration products to the fiber lumens and pores [12–15]. The loss of mechanical strength in BFS based materials has also been reported elsewhere [16] and interpreted as a consequence of carbonation evolution. Furthermore, the interfacial transition zone experiences time dependent modifications such as densification [17], with consequent effects on the mechanical behavior of the fibrous composites.

The toughness is the matrix property that is most often enhanced by the presence of fibers (Table 1). It can be of interest in applications where the cement-based component will be eventually exposed to relatively high dynamic loads (such as earthquakes or wind loads). The plain matrix achieved toughness values between 0.03 and 0.04 kJ/m^2 [6]. The use of 8 wt% sisal CTMP fiber content in BFS improved the toughness of the composite to 0.85 kJ/m^2 at 28 days [11]. The exposure to external environment for 2 years resulted in a toughness reduction to 0.62 kJ/m^2 due to the same mechanisms of composite degradation and fiber embrittlement discussed in the previous paragraph. Similar behavior was observed in the eucalyptus fiber composites, where the reduction of toughness was measured to be approximately 50%.

Studies by Castro and Naaman [18] suggest that more favorable overall mechanical performance can be engineered by the use of hybrid reinforcement with cellulose pulp and discontinuous fibers of non-pulped sisal. These have been achieved by the development of cement-based mortars reinforced with *Agave* fibers with lengths up to 75 mm. Castro and Naaman [18] also showed that the utilization of long fibers with volume fractions between 5 and 11 wt% provided more uniform results.

2.2. Fracture mechanisms

The mechanical properties of FRCs in bending have been studied by several authors [19–21]. Most of these studies have focused on the assessment of the effects of reinforcement with low and high elasticity modulus fibers, such as polypropylene, steel and carbon fibers. The models developed for the prediction of load–deflection behavior are also based on fracture mechanisms observed in notched beam specimens.

Eissa and Batson [21] have used resistance-curve (*R*-curve) experiments to assess the toughness of high strength steel fiber-reinforced concrete notched beams for different fiber types (hooked-end and crimped fibers), and different fiber volume contents (1.0–1.5%). Their studies show that crimped fibers are more effective for increasing toughness because the crimped fibers dissipated more energy than an equivalent volume of hooked-end fibers. Besides, the researchers concluded that the non-linear fracture model based on weight function method can be used to calculate *R*-curves and provide a comprehensive method for evaluating the fracture behavior of high strength steel fiber-reinforced notched beams subjected to flexural loading [21].

Nelson et al. [22] have investigated the fracture toughness of micro-fiber reinforced cement composites (FRCC). They conducted experiments on thin sheet cement composites reinforced with polypropylene (PP), polyvinyl alcohol (PVA) and refined cellulose (RC) fibers. Specimens of FRCC were produced in laboratory using a filter pressed de-watering process, and also by the Hatschek method [23].

The Hatschek process (or wet process) [23] is the most widely used method of fiber–cement production. In this process sheet is produced by the deposition of several layers of fiber–cement. The fibers are oriented preferentially in the longitudinal direction of the sheet. In the case of Hatschek process, a combination of synthetic (PP or PVA) and cellulose fibers was used. The experimental study revealed that the PVA and refined cellulose fibers were able to postpone microcrack formation, thereby delaying final fracture. The PP fibers were not able to provide the same level of reinforcement at the same age due to their weak chemical and frictional interfacial bonds with the cement matrix.

Composite fracture toughness was five times greater than the correspondent matrix fracture toughness for the PP + RC and the PVA + RC fiber-reinforced sheets. The main toughening mechanisms that can take place in the composite include crack bowing or deflection, fiber debonding and pull-out, wake toughening (fiber bridging) and microcrack toughening [24,25].

The *R*-curve behavior requires in general toughening mechanisms which increase in effectiveness with increasing crack length. The toughening mechanisms which results in toughness enhancements in cementitious materials occur largely as a result of crack deflection, crack-bridging and pull-out. Depending on the configuration of the cracks, crack-tip shielding/anti-shielding may also occur due to microcracking [24,25]. Crack deflection occurs in the case of intercrystalline fracture in the matrix of the composites based on cement. It is generally promoted by heterogeneous

Table 1
Properties[a] of cementitious composites reinforced with 8 wt% fiber content [8].

Composite type	Modulus of elasticity (GPa)	Modulus of rupture (MPa)	Toughness (kJ/m^2)	Water absorption (wt%)	Density (g/cm^3)	Permeable voids (% by volume)
Kraft sisal in BFS	6.07 (0.51)	16.8 (1.70)	1.41 (0.22)	29.0 (1.0)	1.39 (0.03)	40.4 (0.6)
Kraft banana in BFS	6.7 (0.6)	21.8 (1.2)	0.59 (0.06)	27.2 (0.6)	1.46 (0.02)	39.7 (1.0)
Kraft *E. grandis* in OPC	11.40 (0.90)	21.4 (0.9)	0.821 (0.110)	20.7 (0.7)	1.60 (0.02)	33.3 (0.6)
Kraft *E. grandis* in BFS	6.64 (0.61)	18.0 (1.4)	0.745 (0.105)	28.0 (1.4)	1.44 (0.04)	40.3 (0.9)

[a] Single standard deviation of sample means indicated in parentheses.

microstructural features, such as anisotropic grain shapes, porosity and second phase such as fibers. In the region near the crack-tip there are intact fibers and debonded fibers. The intact fibers toughen the composite by a combination of crack-bridging and fiber pull-out mechanisms [26]. Both categories of toughening mechanisms give rise to crack-tip shielding and wake process, which are the underlying source of the improved fracture toughness.

3. Material and composite processing

3.1. Material characterization and preparation

Granulated blast furnace slag (BFS) was provided by Companhia Siderúrgica Tubarão (CST), Brazil, as a by-product of pig-iron manufacture, and the chemical characterization follows in Table 2. The BFS was ground to an average Blaine fineness of ~800 m^2/kg and applied as the main component of a clinker-free binder. Ground agricultural gypsum (89% by mass of $CaSO_4 \cdot 2H_2O$) and construction grade hydrated lime (90% by mass of $Ca(OH)_2$) were added as activators in weight proportions of 0.88:0.10:0.02 (BFS: gypsum:lime).

The control binder was produced with the Brazilian Portland cement CP III-RS [28], which is a commercial blend of ordinary Portland cement (OPC), with the replacement of about 66% of ground BFS. The binder also contained the addition of 5% of silica fume with at least 85% by mass of active silica-SiO_2.

Three different types of Brazilian fibrous residue were selected on the basis of their availability and low levels of contamination:

- Waste *Eucalyptus grandis* bleached Kraft pulp, with an estimated availability of 30,000 tonnes/year.
- Sisal (*A. sisalana*) field by-product, with an estimated 100,000 tonnes/year available, equivalent to the amount of commercial sisal production in Brazil.
- Banana (*M. cavendishii*) pseudo-stem fibers, with a potential production of 95,000 tonnes per annum in Ribeira Valley, the main producing area in São Paulo State.

Pulping is a delignification process that contributes to the stability of vegetable fiber in alkaline environments. The non-cellulose components of the fiber can be chemically degraded by alkali attack. The reduction of lignin content has been shown to improve durability of the fiber–cement composites [12]. The fibers from sisal and banana strands were subjected to Kraft (or sulfate) pulping, as detailed elsewhere [29]. The *E. grandis* waste pulp was used as received after undergoing disintegration in tap cold water.

The main physical attributes of the pulps have been described in earlier work [29]. These are summarized in Table 3. Note that the Kappa number is an indication of residual lignin content in chemical pulps. The method is related to the consumption of permanganate (i.e., the oxidation of the residual lignin in pulp). An estimation of residual lignin within these reinforcement fibers is important because of the aging of natural fibers that occurs in contact with alkaline media such as ordinary Portland cement [30].

The Canadian Standard Freeness (CSF) is an arbitrary measure of the drainage properties of pulp suspensions. It is associated with the initial drain rate of the wet pulp pad during the de-watering process [31]. Fiber length was determined using a Kajaani FS-200 automated optical analyzer. The average length was calculated on a length-weighted basis, which is less influenced by the proportion of fines [32]. The aspect ratio is the ratio of the average length of the fiber to the average fiber width.

Pulped fibers were preferred for the production of composites using the slurry vacuum de-watering technique that was used for the production of fiber–cement in this work. This enabled a crude simulation of an industrial process at the laboratory scale. During the de-watering stage, the pulp forms a net that is responsible for the retention of cement grains. This network of pulp also enables a homogeneous planar (2-D) distribution of short fibers within matrix.

Table 2
Chemical composition of granulated blast furnace slag (wt%) [27].

Loss on ignition	1.67	SO_3	0.15
SiO_2	33.78	Na_2O	0.16
Al_2O_3	13.11	K_2O	0.32
Fe_2O_3	0.51	S^{2-}	1.14
CaO	42.47	Free CaO	0.1
MgO	7.46	Insoluble residue	0.53

Table 3
Pulp and fiber properties.

Property	Sisal	Banana	*E. grandis*
Kappa number[a]	32	45	6.1
Canadian Standard Freeness[b] (mL)	650	222	685
Fiber length (length weighted)[c] (mm)	1.65	1.95	0.66
Fiber width average[d] (μm)	13.5	15.3	10.9
Aspect ratio	122	127	61

[a] Appita P201 m-86 [33].
[b] AS 1301.206s-88 [34].
[c] Kajaani FS-200.
[d] Average of 20 determinations by scanning electron microscopy (SEM).

3.2. Composite production

Composites with fiber mass fractions of 8% (approximately 10% by volume content) were prepared in the laboratory using the slurry vacuum de-watering technique [35]. The selection of fiber content was based on optimum levels found in a similar study [29]. Binder was added to the appropriate amount of fiber, already dispersed in water, to form a slurry with approximately 20% of solid materials. After stirring for 5 min, the slurry was transferred to an evacuable ~130 × 130 mm casting box placed under an initial vacuum (~60 kPa gauge) for removal of excess water, forming a solid surface. The moist pad was tamped flat, and the vacuum was reapplied for 2 min.

The pad was then transferred to an oiled steel plate and pressed at 3.2 MPa for 5 min. After pressing, the thickness of the pad was 15 mm. Upon completion of consolidation, the metallic plate was removed and the pads sealed in a plastic bag to cure in saturated air at ambient temperature for 3 days. In order to optimize hydration the curing continued by placing pads in water bath for additional 4 days. The pads were then air cured in a laboratory environment until they were tested, approximately two years after production. In the case of sisal pulp in BFS series, the mechanical tests were also carried out on specimens that were aged for 9 months.

It was observed in a previous work, as described by Savastano et al. [11], that there was a clear decrease in the modulus of rupture (MOR) of the composites, of about of 30%, in comparison with the correspondent series tested at 28 days of age. However, there was a stabilization of the composite mechanical properties for aging durations between 9 and 24 months. This can be attributed to the absence of degradation agents due to natural weathering in the internal environment.

3.3. Experimental procedures

3.3.1. Resistance-curve experiment

The resistance-curve experiments were performed on single-edge notched bend (SENB) specimens with thickness (B) of

~7.5 mm, width (W) of ~12.5 mm and length of 65 mm. The initial notch-to-width ratio (a_0/W) was ~0.25. The specimens were prepared by starting from the raw pads that were produced as described in the previous section. The specimens were prepared using a diamond cut off wheel, prior to grinding and final polishing of the specimen sides with diamond paste.

Experiments were conducted under three-point bend loading, with a span of 50 mm. The resistance-curve experiments were performed in an Instron model 8872 servo-hydraulic testing machine, after pre-cracking under far-field compression to introduce sharp pre-cracks at the notch roots [36]. The resistance-curve experiments were then carried out on the specimens after hygroscopic stabilization in a laboratory environment with a relative humidity of ~40–50% and a temperature of ~25 °C.

The specimens were loaded monotonically in incremental stages that corresponded to a stress-intensity-factor range (K) increase rate of 0.05 MPa $\sqrt{m}$. This was achieved at a ramp rate of 2 N/s. The specimens were then unloaded to examine their sides for evidence of possible crack growth. This was continued until crack growth was detected in an insitu Questar QM100 telescope (Questar, New Hope, PA, USA) connected to a video monitoring system. This enabled crack length measurements with a resolution of ~2.5 μm.

The insitu Questar telescope was used to study the crack/microstructure interactions that give rise to resistance-curve behavior. This was continued until unstable crack growth/fracture occurred during incremental loading. The calculations of K were obtained from an expression in the ASTM E399-90 code [37]. This gives:

$$K = \frac{PSf\left(\frac{a}{W}\right)}{BW^{1.5}} \tag{1}$$

where

$$f\left(\frac{a}{W}\right) = \frac{3(a/w)^{0.5}\left[1.99 - (a/W)(1-a/W)(2.15 - 3.93a/W + 2.7a^2/W^2)\right]}{2(1+2a/W)(1-a/W)^{1.5}} \tag{2}$$

P is the applied load, B is the specimen thickness, W is the specimen depth (width), S is the span, and a is the crack length. More details about the equation for the calculation of the geometry/compliance function $f(a/W)$ can be obtained in the ASTM E399-90 [37].

After specimen failure, the fracture surfaces of as received fractured specimen were examined in a field emission gun (FEG) scanning electron microscope (SEM). This was done using a secondary electron (SE) imaging mode. The SEM was equipped with an energy dispersive X-ray spectroscopy (EDS) system (Princeton Gamma-Tech – PGT) that was used for high-resolution spatial elemental analyses, as well as point analyses from the sample surface. The specimens were coated with a 35 nm layer of Au (Ion Beam Sputterer – IBS/TM 200S) prior to SEM/EDS analyses.

3.3.2. Fatigue crack growth

The fatigue crack growth experiments were performed on the same type of single-edge notched bend (SENB) specimens. The initial notch-to-width ratio was ~0.25 that was the same used in the resistance-curve tests. The SENB specimens were pre-cracked under cyclic far-field compression loading [36] at a stress ratio $R = K_{min}/K_{max}$, of 10. This was done to introduce sharp pre-cracks into the notch root regime.

Subsequently, the specimens were oriented in three-point bend loading, and subjected to cyclic loading in an Instron 3369 servo-hydraulic testing machine (Instron, Canton, MA, USA).

The fatigue crack growth experiments were performed at a stress ratio, $R = K_{min}/K_{max}$, of 0.1. The initial cyclic stress ranges were increased in steps of ~5–10% until stable crack growth was observed with the same Questar telescope that was used in the resistance-curve experiments. The crack lengths and crack/microstructure interactions were monitored using the Questar QM100 telescope (Questar, New Hope, PA, USA) until catastrophic failure occurred.

Finally, the through-thickness nature of the cracks, and the final crack lengths, were checked by comparing the actual crack profiles with the measurements of crack lengths from the sides of the specimens. The underlying fatigue fracture modes were also studied using SEM techniques that were similar to those used in the resistance-curve experiments.

4. Micromechanical modeling

4.1. Crack-bridging under monotonic loading

Since crack-bridging was commonly observed in this work (Fig. 1), it is of interest to analyze its role of crack-bridging during crack growth under monotonic loading. An energy approach [24] may be used to explain the toughening due to crack-bridging by ductile fibers or ligaments. The toughening of the brittle matrix due to small-scale bridging by ductile fiber reinforcement may be idealized using an elastic–plastic spring model, as proposed by Budiansky et al. [38] and Li and Soboyejo [39].

For small-scale bridging, in which the size of the bridging zone is much smaller than the crack length [4], the extent of ductile phase toughening may be expressed in terms of the maximum stress intensity factor the material can sustain before failure (fracture toughness). Under small-scale bridging (SSB) conditions (bridge length $\leqslant$ 0.5 mm), the fracture toughness of the composite, K_c, can be expressed as the sum of the matrix fracture toughness, K_m, and the toughening component due to small-scale crack bridging, ΔK_{ssb}. The fracture toughness of the fiber-reinforced composites may thus be estimated from Eq. (3), as stated by Soboyejo [24]:

$$K_c = K_m + \Delta K_{ssb} = K_m + \left(\frac{2}{\pi}\right)^{0.5} \alpha V_f \int_0^L \frac{\sigma_y}{x^{0.5}}\,dx \tag{3}$$

where α is the constraint/triaxiality factor (typically between 1 and 3 and taken to be ~1 in this study) [4,5], V_f is the volume fraction of ductile phase, L is the length of the bridging ligament, σ_y is the uniaxial yield stress, and x is the distance from the crack-tip as detailed by Savastano et al. [11].

For large-scale bridging conditions the length of the bridging zone is comparable to the overall crack size. In this case, the toughening increment (ΔK_{lsb}) is given by Eq. (4) [5,39–41]:

$$\Delta K_{lsb} = V_f \int_L \alpha \sigma_y h(a,x)\,dx \tag{4}$$

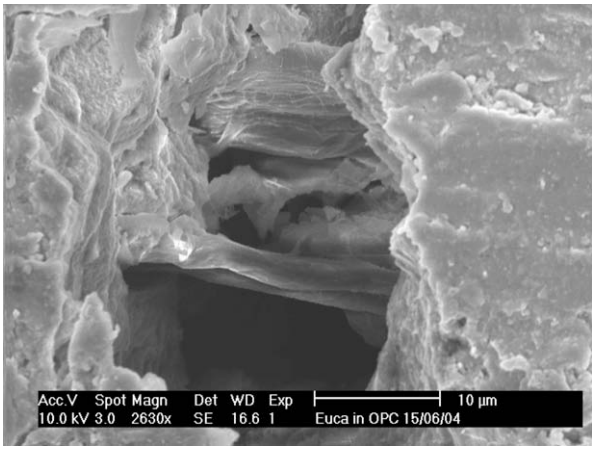

Fig. 1. SEM image of eucalyptus pulp in OPC matrix. Bridging fiber in the cracked fracture.

Table 4
Summary of Fett and Munz [42] parameters for SENB specimen subjected to weighted crack-bridging fractions.

v	μ				
	0	1	2	3	4
0	0.4980	2.4463	0.0700	1.3187	−3.067
1	0.5416	−5.0806	24.3447	−32.7208	18.1214
2	−0.19277	2.55863	−12.6415	19.7630	−10.986

where $h(a,x)$ is the weighting function for the bridging tractions given by Fett and Munz [42]. This is given by Eq. (5):

$$h(a,x) = \sqrt{\frac{2}{\pi a}}\frac{1}{\sqrt{1-\frac{x}{a}}}\left(1+\sum_{(v,\mu)}\frac{A_{v\mu}\left(\frac{a}{W}\right)}{\left(1-\frac{a}{W}\right)}\left(1-\frac{x}{a}\right)^{v+1}\right) \quad (5)$$

where the coefficients ($A_{v\mu}$) are given in Table 4 for a single-edge notched bend (SENB) specimen.

4.2. Crack-bridging under cyclic loading

The fatigue crack propagation behavior of many materials can be divided into three categories. A transient occurs in which da/dN diminishes upon crack growth, at fixed stress amplitude, followed by a steady-state region in which da/dN remains constant, where N is the number of loading cycles. When this behavior is obtained, the fibers are observed to remain largely intact upon matrix crack growth and bridge the crack surfaces. However, these results depend strongly on length and diameter distributions of the fibers as well as of its durability into composites.

Under cyclic loading in the composite reinforced with vegetable pulp fiber it can be observed relative motion between fibers and matrix during matrix crack opening/closing, characterized by a friction law, with a sliding stress. These composites exhibit features that cannot be characterized in accordance with the Paris law that governs only matrix behavior [48]. For example, the Paris law does not take accounts that the bridging tractions undergo reversals when the cyclic loads are reversed.

The bridging tractions undergo reversals that have been modeled by McMeeking and Evans [48] for fiber-reinforced composites subjected to fatigue loading at a stress ratio, R, of zero. Their results suggest that the effective bridging stress-intensity-factor range, ΔK_{eff}, corresponds to the crack-bridging at the arithmetic mean stress, σ_{mean}. This gives:

$$\Delta K_{eff} = \Delta K_{app} - K_b(\sigma_{mean}) \quad (6)$$

where ΔK_{app} is the applied stress-intensity-factor range and K_b (σ_{mean}) is the bridging stress intensity factor at the arithmetic mean stress, σ_{mean}. The measured fatigue crack growth rate data will be presented in terms of ΔK_{app} or ΔK_{eff} described above.

5. Results and discussion

5.1. Resistance-curve behavior

The resistance-curves obtained for the vegetable fiber–cement composites are presented in Figs. 2–4. Table 5 contains the main information extracted from the resistance-curves for each tested sample: maximum ratio between the stable crack length and the specimen depth (a/W), initial and final stress intensity factors (K_0 and K, respectively).

Stable crack growth initiated at a stress intensity factor, K_0, that varied from 0.6 MPa $\sqrt{m}$ (eucalyptus pulp in OPC matrix) to 0.90 MPa $\sqrt{m}$ (banana pulp in BFS matrix). The average amount of stable crack growth (Δa) resulted in a/W ratio around 0.4, and the average stress intensity factor reached ~1.3 MPa $\sqrt{m}$.

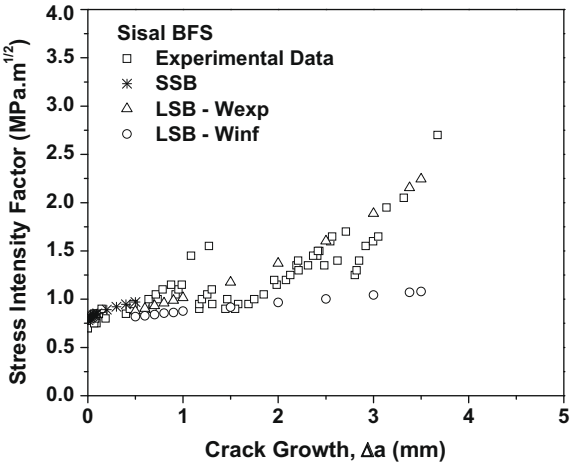

Fig. 2. Experimental R-curves of the BFS cement paste reinforced with sisal pulp with 9 months and 2 years of age and calculated curves using small and large-scale bridging models (SSB and LSB, respectively). The LSB model was simulated with experimental depth (W_{exp}) and infinite (W_{inf}).

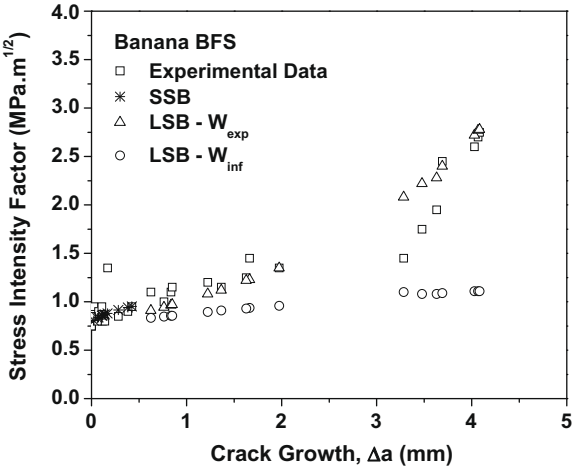

Fig. 3. Experimental R-curves of the BFS cement paste reinforced with banana pulp with two years age and calculated curves using small and large-scale bridging models (SSB and LSB, respectively). The LSB model was simulated with experimental depth (W_{exp}) and infinite (W_{inf}).

Thirteen tests were performed in the present study. The anomalous behavior was registered for some specimens in the end of the curve. For this reason the final part of curve was rejected considering a crack extension until 4 mm. For example, two experimental curves reached stable crack growth (Δa) of 5 mm, corresponding to $K > 4$ MPa $\sqrt{m}$ and $a/W \sim 0.67$. Such a different trend was not considered as representative of the intrinsic behavior of the composite but as the influence between the fracture process zone and specimen boundary. It is important that the crack-bridging zone to be small enough as compared to the specimen dimension for the resistance-curve to be a characteristic of the material.

On the other hand, heterogeneous distribution and different lengths of the fibers into the cement matrix has had an influence on R-curve behavior of the composites. Table 3 evidences the greater average lengths of sisal and banana fibers in comparison to eucalyptus fiber. The fibers from sisal and banana strands were subjected to crude Kraft pulping in the laboratory scale [29] while the *E. grandis* was the waste pulp from papermaking industry. Long length could disturb the homogeneous distribution of the vegetable pulp in high volume content into the cementitious matrix.

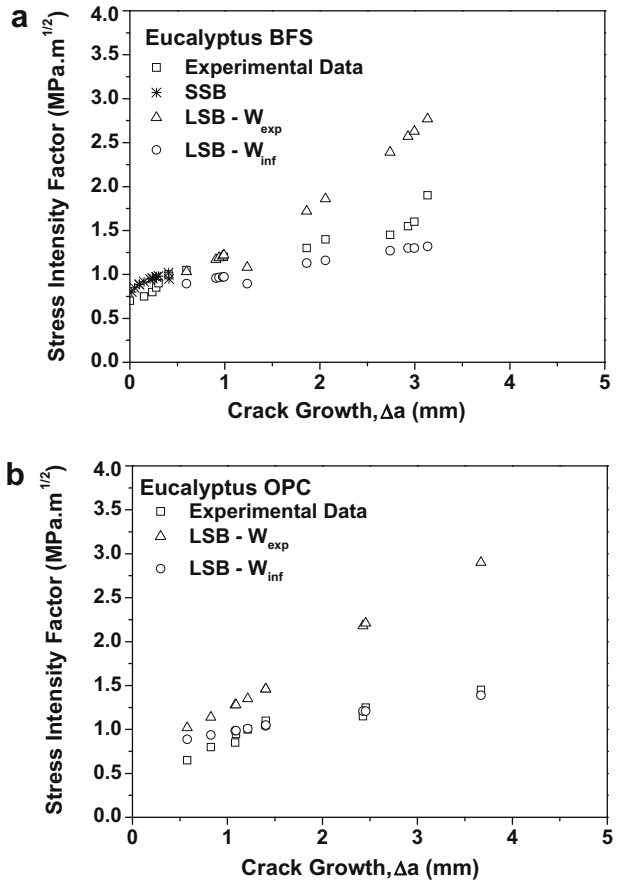

Fig. 4. Experimental *R*-curves of composites reinforced with eucalyptus pulp with two years age and calculated curves using small and large-scale bridging models (SSB and LSB, respectively). The LSB model was simulated with experimental depth (W_{exp}) and infinite (W_{inf}): (a) BFS and (b) OPC cement paste.

Table 5
Main information from the resistance-curves of vegetable fiber–cements.

Series	Specimen #	K_0 (MPa $\sqrt{m}$)[a]	K (MPa $\sqrt{m}$)	a/W
1-Sisal in BFS	1–1	0.80	1.40	0.479
	1–2	0.80	1.50	0.448
	1–3	0.70	4.10[b]	0.671[b]
	1–4	0.80	1.65	0.500
2-Banana in BFS	2–1	0.75	0.85	0.266
	2–2	0.90	1.45	0.387
	2–3	0.75	4.25[b]	0.666[b]
	2–4	0.75	0.90	0.266
	2–5	0.85	1.35	0.270
3-Eucalyptus in BFS	3–1	0.80	1.20	0.349
	3–2	0.70	1.15	0.330
	3–3	0.70	1.90	0.506
4-Eucalyptus in OPC	4–1	0.60	1.45	0.561

[a] $a_0/W \sim 0.25$.
[b] Values not considered as representative of the intrinsic behavior of the composite.

Fiber cement reinforcement with *E. grandis* waste pulp, due to short length of this fiber (Table 3), presented a fracture process less stable than the composites with sisal and banana fibers. The length of fiber is one of main factors that influence on the process by which load transferred from the matrix to fibers and interfere in the bridging effect of the fibers across the matrix cracks (debonding and pull-out), which occurs at a more advanced stage of loading.

It is of interest to compare the results of the current study to prior reports of fracture toughness/resistance-curve behavior in cementitious materials. In the present work, the random distribution of short fibers makes the modeling of crack-bridging more challenging. Similar resistance-curve behavior was observed in cement matrices reinforced with different types of fibers, such as carbon, steel and polypropylene. These include studies by Eissa and Batson [21] and Banthia and Sheng [44]. Banthia and Sheng [44] used the *R*-curve approaches to study the effects of polypropylene fibers (4 μm diameter, 6 mm long, E = 1.41 GPa) as reinforcements in a cement paste based matrix. Following reinforcement with up to 3% by volume of fiber content, the improvement of the composite toughness was significant, compared with the un-reinforced matrix. At this level of reinforcement, the effective final crack length, a_{eff}, (measured using compliance method) varied from 8 to 8.45 mm ($W \sim 25$ mm) and values for K_I reached ~0.55 MPa $\sqrt{m}$.

Nelson et al. [22] presented a range of values from 0.2 to 0.3 MPa $\sqrt{m}$, respectively, for the critical stress intensity factor (K_0) of hardened cement paste (HCP) for cement specimens that contain silica fume and have a water/cement ratio of 0.3. In the same study, refined cellulose pulp was able to delay the formation of micro-cracks in the composites. For V_f equal to 10%, the K_0 value was between 0.7 and 0.8 MPa $\sqrt{m}$, which is comparable to the interval reached in the present study (see Table 5).

5.2. Comparison of bridging predictions with experimental results

The presence of vegetable micro-fibers has a significant effect on the fracture toughness, and on the extent of stable crack growth

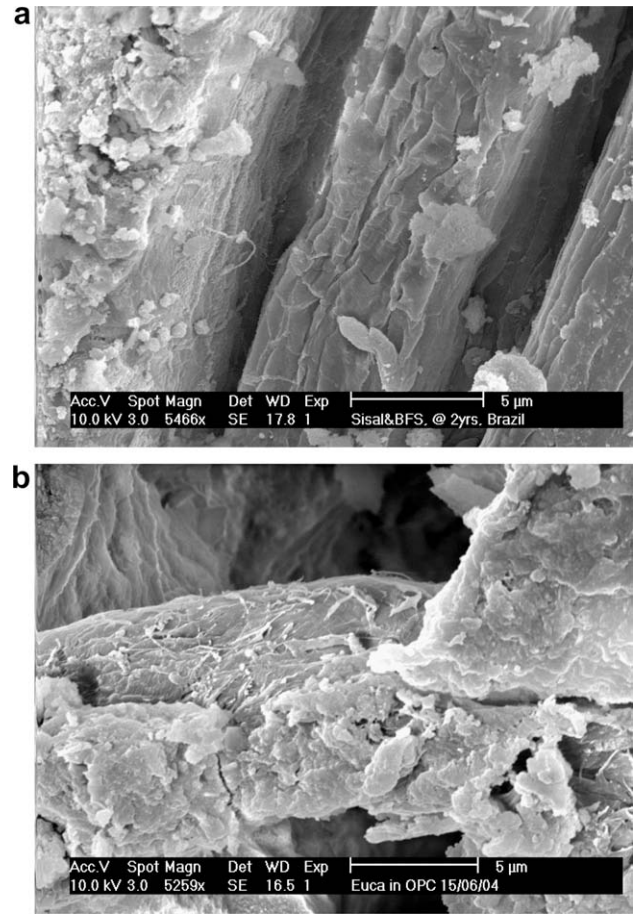

Fig. 5. (a) SEM image of sisal pulp in BFS matrix. Fiber completely debonded from the cement matrix. (b) SEM image of eucalyptus pulp in OPC matrix. Pulled out fiber with indication of good adhesion due to matrix incrustations.

observed in this cement-based material (Figs. 2–4). For a given volume of reinforcement, the fiber spacing is inversely proportional to the stress required to cause cracking [43].

The measured resistance-curve behavior in Figs. 2–4 can be compared with the predicted based on the micromechanical models presented earlier in Section 4. As in previous work [5,11],

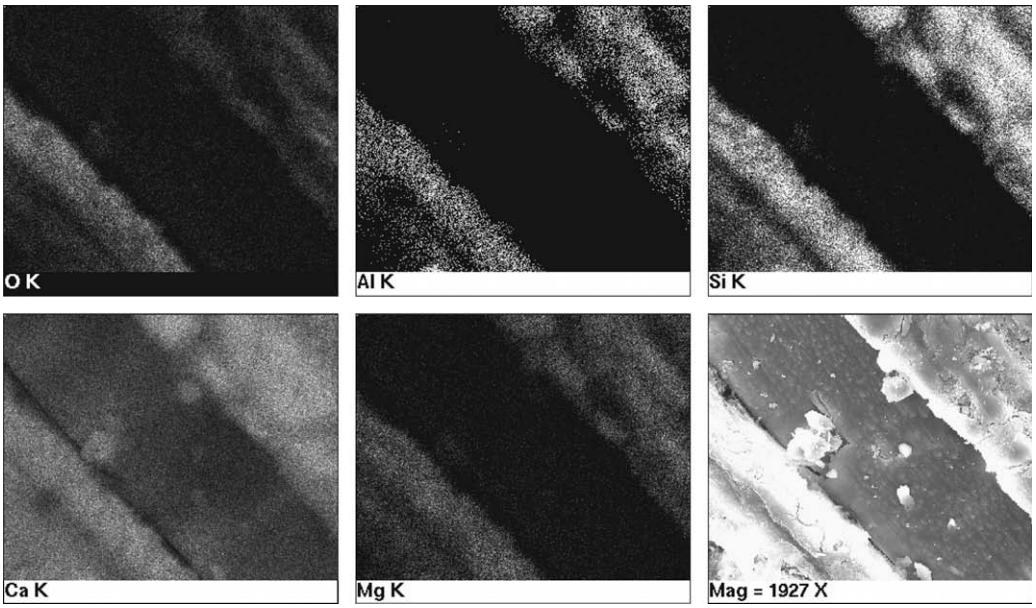

Fig. 6. Elemental map by EDS of banana pulp in BFS. There is some crystal growth that destroys the integrity of the fibers. The concentration of Ca in the surface of the fiber indicates presence of portlandite.

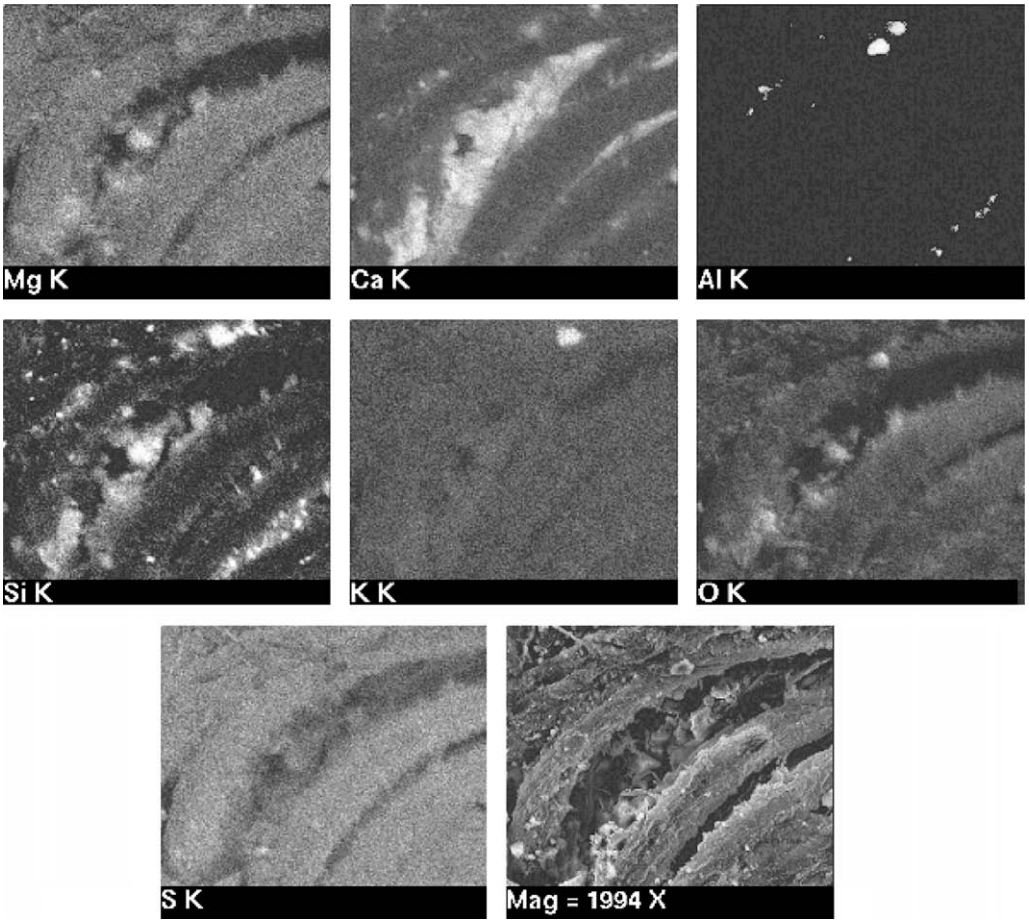

Fig. 7. Elemental map by EDS of sisal pulp in BFS. The space between individual fibrils is occupied by hydration products.

small-scale bridging (SSB) was presumed to occur for crack growth, Δa, less than ~0.5 mm, and large-scale bridging (LSB) was assumed for $\Delta a \geqslant 0.5$ mm. Hence, the predictions of the initial portion of the curve, Figs. 2–4 were based on Eq. (3), while the predictions of toughening in the LSB-regime were based on Eq. (4). Typical values of crack-bridging parameters, such as bridge length, L, and fiber volume fractions were estimated by quantitative image analyses of side profiles.

Using the average initiation toughness, K_0, of 0.76 MPa $\sqrt{m}$, the K levels corresponding to each increment of crack growth can be estimated from the sum of K_i and the toughening increment due to crack-bridging, ΔK_b. The resistance-curve is, therefore, given simply by $K_0 + \Delta K_{ssb}$ for small-scale bridging and $K_0 + \Delta K_{lsb}$ for large-scale bridging. In the case of small-scale bridging, the constraint/triaxiality factor was assumed to be ~1, and the value of V_f was estimated to be 0.23. The fiber tractions were assumed to correspond to ~30 MPa, which corresponds roughly to the average level of tensile strengths of natural fibers [45] after exposure to alkaline media. According to prior work [7], the composite strengths were found to be reduced by about half, after one year of interactions between the natural fibers and the cement matrix.

In the predictions for small-scale bridging, the value reached for the overall increment, ΔK_{ssb} = 0.212 MPa $\sqrt{m}$, is in good agreement with the experimental measurements. This behavior is in accordance with a previous work by Kung et al. [4] regarding the predicted resistance-curve.

For the large-scale bridging (LSB) prediction, the values for α, V_f, σ_y and L were adopted to be as those used for the SSB predictions. A comparison of the predictions obtained from Eq. (4) and the measured LSB resistance-curve is also presented in Figs. 2–4. The experimental values of the stress intensity factor reached ~1.9 MPa $\sqrt{m}$ for the formulation eucalyptus in BFS corresponding to stable crack growth (Δa) of 3.1 mm and to a/W = 0.51. The LSB model also predicts very well the overall trends of these experimental results (~2.0 MPa $\sqrt{m}$ to approximately the same a/W value).

The resistance-curves are specimen dependent. It is, therefore, important to obtain estimates of fracture toughness that do not depend so strongly on crack length or specimen geometry. The estimates would represent the true intrinsic toughness of the composites, which would normally require the testing of very large specimens. Such estimates of the intrinsic composite fracture toughness can be achieved by artificially increasing the specimen width, W, such that $W \to \infty$. The function $h(a,x)$ is found to approach an asymptotic value when this is done (Figs. 2–4). From Eq. (4), this gives an estimated intrinsic fracture toughness value of ~1.2 MPa $\sqrt{m}$ for the composite with sisal and banana pulp. The intrinsic fracture toughness reached the value of ~1.3 MPa $\sqrt{m}$ and ~1.4 MPa $\sqrt{m}$ for the BFS and OPC cement, respectively, reinforced with eucalyptus pulp. The difference between the simulations with real value of W (large-scale bridging model) and with $W \to \infty$ (intrinsic toughness) shows the influence of the specimen dimensions, especially for higher values of Δa (Figs. 2–4).

Both SSB and LSB models capture the general trends of the measured resistance-curves and the values predicted by the models are compatible with the corresponding experimental measurements. These results attest the appropriate application of the models under consideration in spite of the heterogeneity of the material, the random distribution of the reinforcement and the degradation of ligaments bridges between the cement matrix and the natural fibers as discussed by Savastano et al. [11].

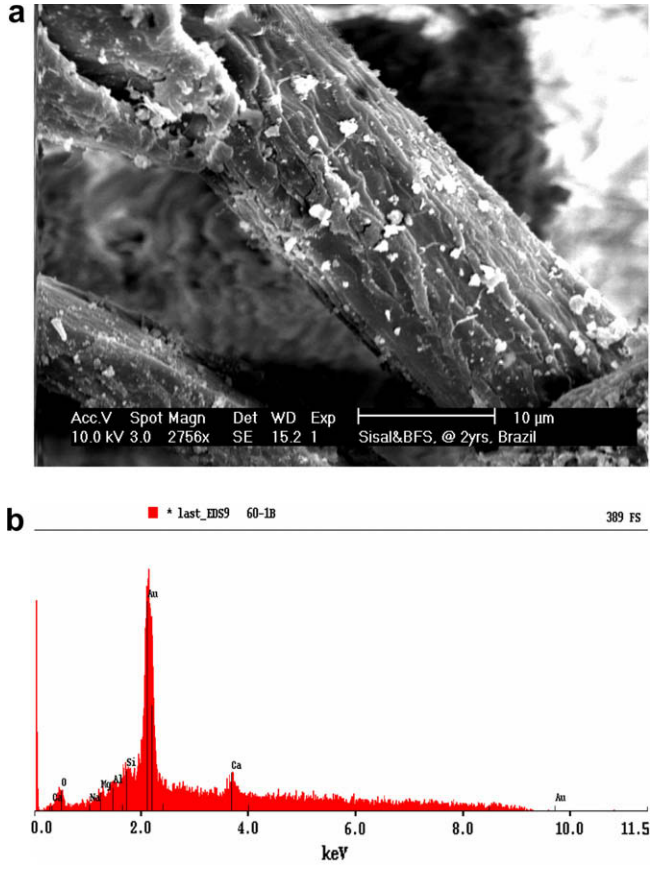

Fig. 8ab. (a) SEM image of sisal pulp in BFS matrix and (b) EDS analysis of the fiber surface. Fiber not covered with hydration products as an indication of poor bonding. Fiber not destroyed by the cement environment.

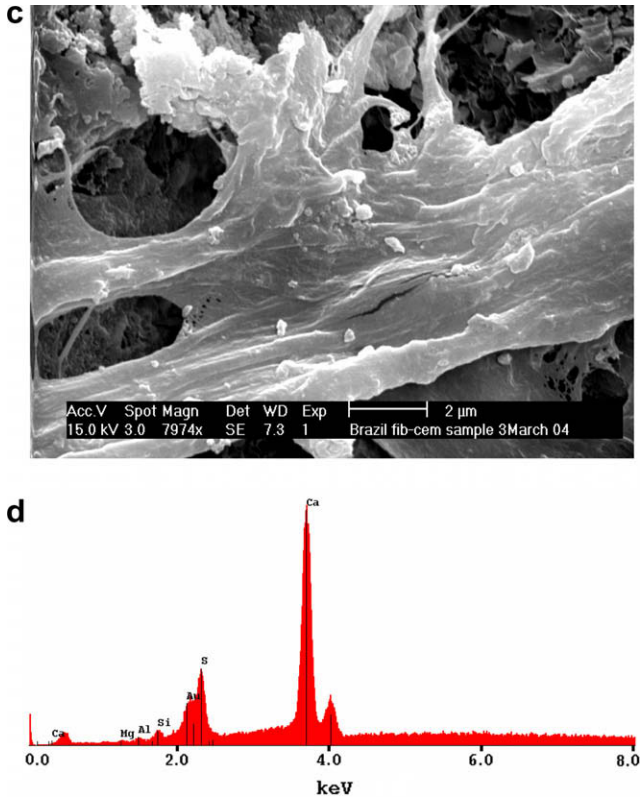

Fig. 8cd. (c) SEM image of eucalyptus pulp in BFS matrix and (d) EDS analysis of the fiber surface. Ca and S compounds are likely to be present on fiber surface.

Note that it was not possible to define the initial crack growth from the experimental tests for OPC cement paste reinforced with eucalyptus pulp (Fig. 4b), because of the instability of the crack propagation due to short length of this fiber. As consequence, the curve using small-scale bridging model (SSB) was not obtained.

It can be also seen that the LSB prediction with $W \rightarrow \infty$ (intrinsic toughness) fitted better with experimental data from the BFS and OPC cement paste reinforced with eucalyptus pulp (Figs. 4a and 4b) than one with real value of W.

The SSB and the LSB models suggest that improved fracture toughness/resistance-curve behavior can be engineered by improving fiber strength, increasing bridge length and modifying fiber volume fraction up to optimum levels.

The development of coatings or surface treatments for natural fibers could be implemented to avoid the reduction of the initial fiber strengths by fiber/matrix interactions [13,46]. Another possibility could be the modification of the cement matrix, mainly by reducing pH of pore solutions, which appears to be aggressive to the fiber. That could be achieved by the use of blended cements, by pozzolanic or slag additions or by the use of polymer modified cement systems [7,45]. Additionally the production of composites with lower permeability and/or protected by surface treatment based on water repellent could also contribute to the durability and consequently to the stable mechanical performance of fiber–cement composites under various environmental conditions, which might be encountered during service life of structures built of such materials [45].

5.3. Microstructure analysis

Microscopic observations of control specimens and specimens subjected to various chemical and physical environments provide valuable information on mechanisms of failure. This can be then used to develop new designs and curing regimes for cement–fiber composites, which could reduce some of the deleterious effects studied. Therefore, microstructure characterization provides insight into macro-properties of material under specific conditions.

5.3.1. Fiber–matrix interfacial transition zone

One component of toughening mechanisms that is predominant in cellulose pulp cement composites is fiber debonding. It is due to the volume variation of the natural fiber depending on its moisture

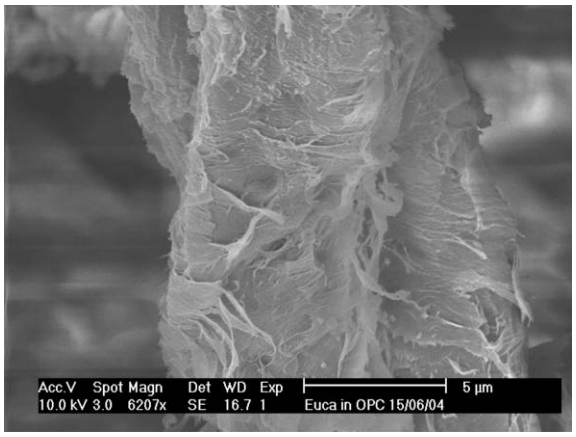

Fig. 9. SEM image of eucalyptus pulp in OPC matrix. Detail of the fiber surface.

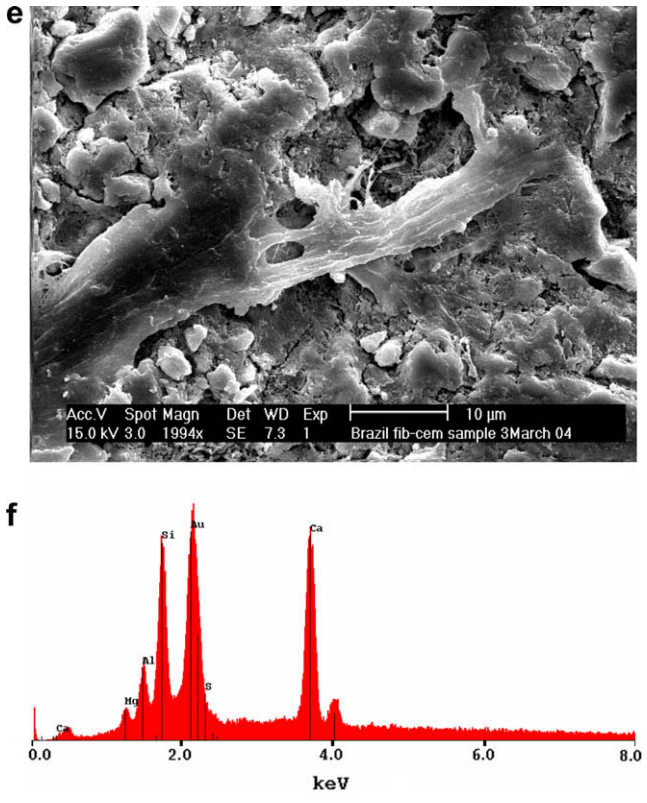

Fig. 8ef. (e) SEM image of eucalyptus pulp in BFS matrix and (f) EDS analysis of the matrix fracture surface. Ca and Si peaks of similar magnitude denote hydration products without concentration of portlandite.

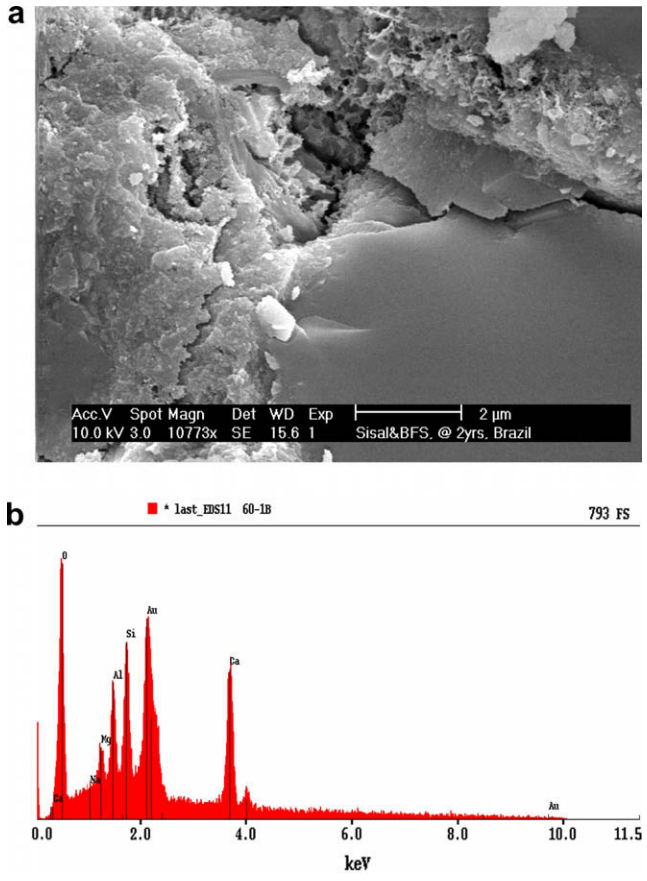

Fig. 10. (a) SEM image of the BFS matrix and (b) EDS analysis of the hydration products (left hand side). The main compounds of slag matrix are present with no indication of calcium accumulation.

content and tension state. A demonstration of fiber debond can be observed on a fractured composite surface. Fig. 5a is indicative of fiber debonding with the correspondent reduction in tension transferring from cracked matrix.

The incrustation of matrix in fiber surface is a demonstration of good interaction between both phases with the consequent absorption of energy during fiber pull-out as shown in Fig. 5b.

The micrographs in Fig. 6 show some alterations on the surface of fibers, especially crystal growth that destroys the integrity of fibers probably due to the crystallization of portlandite (calcium hydroxide). The matrix shows small oscillation in chemical composition mainly in Ca/Si ratios and presence of Mg. There is no indication of the concentration of hydration products in relation to the proximity of the fiber.

Elemental maps in Fig. 7 present spatial distribution of major chemical elements at the interfacial transition zone (ITZ) between fibers and cementitious matrix. It can be observed in this micrograph that the spaces between individual fibrils are occupied by precipitated Ca, Si and Mg compounds. This phenomenon can be associated to the fiber mineralization as inferred by Bentur and Akers [15].

5.3.2. Fiber surface

Fig. 8a shows the sisal fiber pulled-out from the cement matrix with no significant accumulation of hydration products in the fiber surface as confirmed in the correspondent EDS analysis, Fig. 8b. This demonstrates poor bonding between phases as previously denoted in Fig. 5a. However, there is no visual evidence of decomposition of the reinforcing phase due to the good aspect of the surface of the fiber into the aged composite.

The Fig. 8c shows a SEM of eucalyptus pulp in BFS matrix. The correspondent EDS analysis applied to BFS paste reinforced with eucalyptus pulp shows incidence of Ca and S compounds (portlandite and/or gypsum) in the surface of the fibers as in Fig. 8d. Petrifaction is the phenomenon that may be associated to this fact when the fiber voids are filled with some hydration products with the consequent reduction of the fiber tenacity, Fig. 8e [12,15]. The same analysis in the fracture surface of the matrix (Fig. 8f) indicates incidences of Ca and Si of similar magnitude. Peaks of S, Mg and Al are also present in the sample as one could expect based on the composition of the slag and its chemical activators.

Fig. 9 attests the integrity of the fiber even after been immersed for approximately two years in the ordinary Portland cement matrix, although some degradation in the surface of the fiber is evident. Such a superficial decomposition of the fiber could be understood by the peeling-off reaction with the consequent depolymerization of the cellulose molecules as proposed by Pavasars et al. [47].

5.3.3. Matrix

Fig. 10a depicts the cementitious matrix with the interfacial zone between the slag anhydrate grain and the hydration products. Fig. 10b presents the EDS analysis of the hydration products (left hand side of the micrographs) and indicates no high concentration of Ca in relation to Si or to the other compounds (especially Mg and Al).

5.3.4. Bridging effect

Fig. 1 shows the interaction between eucalyptus pulp and OPC matrix. Fig. 1 depicts the fiber crossing the gap generated in the

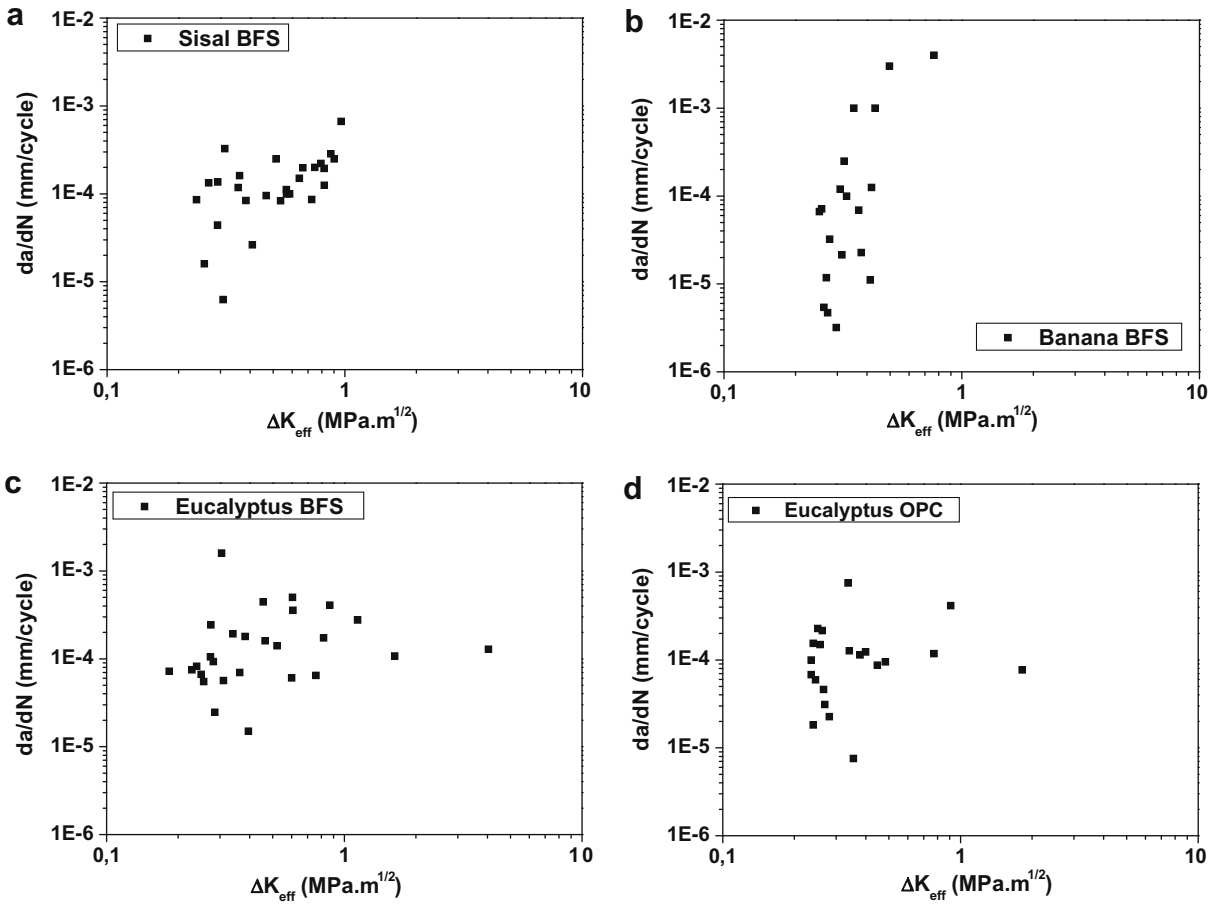

Fig. 11. Fatigue crack growth rate data. (a) Sisal BFS (b) Banana BFS (c) Eucalyptus BFS and (d) Eucalyptus OPC.

cracked matrix which is associated to the bridging effect. At this portion of the tensioned composite all the stresses are transferred from the matrix to the fiber that will be responsible for carrying the increased loads. In the case of short fibers that were randomly distributed in the matrix, the efficiency of the bridging elements tends to be comparatively lower in comparison to that in composites with continuous and aligned reinforcements [43].

5.4. Fatigue crack growth

Fig. 11 depicts the diagrams of the crack growth rate, da/dN, and effective amplitude of applied stress intensity factor, ΔK_{eff}, of the composites reinforced with sisal pulp, banana pulp and *E. grandis* pulp. Fatigue crack growth was observed to occur in three stages: an initial decelerated growth, a steady-state growth, and a final catastrophic crack growth. In the case of the composites reinforced with sisal and banana pulps, most of fatigue life was spent in the second stage of steady-state crack growth (Figs. 11a and 11b). The aspect ratio of the fibers (Table 3) was important to guarantee a major stability to the crack growth under cycling loading. The large lengths of the filaments constituents of the banana and sisal pulps, as compared with *E. grandis* pulp, helped to promote frictional stress transfer mechanisms from matrix to fibers, i.e., pull-out mechanism.

Fiber cement reinforced with *E. grandis* waste pulp exhibited faster fatigue crack growth rates than the composites reinforced with sisal and banana pulps (Figs. 11c and d). A similar reduction in crack growth resistance was also observed in the *R*-curve experiments on the composites reinforced with *E. grandis*.

The crack/microstructure interactions also revealed that fatigue crack growth in the composites occurred via matrix cracking, crack deflection around fibers, and crack-bridging by uncracked fibers and ligaments. The observed fiber-pull-out also suggests a mechanism of crack growth via the degradation of bridging tractions that can occur under cyclic loading. These give rise to inelastic stresses that can lead to crack growth in ceramic materials, as proposed by Ritchie [49].

6. Concluding remarks

This paper presents the results of a combined experimental and theoretical study of fatigue crack growth and resistance-curve behavior in natural fiber-reinforced cementitious composites. Sisal and banana waste residues converted to Kraft pulps and residual eucalyptus bleached pulp were successfully employed as reinforcement of cement-based matrices. Salient conclusions arising from this study are presented below.

1. Blast furnace slag and ordinary Portland cement-based pastes reinforced with non-conventional Kraft pulps exhibited initiation fracture toughness levels between ~0.6 and 1.9 MPa $\sqrt{m}$, respectively. This fracture toughness is considered significantly greater than that of the plain cement paste (0.2–0.3 MPa $\sqrt{m}$) [22].
2. Toughening in the natural fiber-reinforced composites occurs largely as a result of crack-bridging. The trends in the predictions of resistance-curve behavior obtained from small- and large-scale bridging models are in agreement with the corresponding experimental measurements.
3. The intrinsic toughness of the natural fiber–cement composites reinforced with sisal, banana and eucalyptus fibers was estimated to be between ~1.2 and 1.4 MPa $\sqrt{m}$. This represents the true specimen-independent fracture toughness value of the material.
4. Evidence of crack-bridging and fiber pull-out was observed on the fracture surfaces of the *R*-curve specimens. The intense interaction between the cement matrix and the cellulose pulps can be inferred from evidence of fiber incrustation or mineralization by cementitious hydration products. However, the fibers are well preserved, even after two years of exposure to the cement environment.
5. The composites reinforced with sisal and banana pulps exhibited clearly stable rising *R*-curve behavior that correspond to stable fatigue crack growth, while those reinforced with *E. grandis* waste pulp had only limited fracture and fatigue crack growth resistance. The potential reason for the difference in behavior was associated to the aspect ratio and length of the fibers.
6. Stable fatigue crack growth in natural fiber cementitious composites is attributed to the degradation of bridging zones, as in ceramic matrix composites. The cyclic degradation is thought to give rise to inelastic deformation and crack growth ahead of the crack-tip.

Acknowledgments

The research reported in this paper is supported by the Division of Civil and Mechanical Systems (CMS) and the Division of Materials Research of the National Science Foundation (Grant Nº CMS 0303492 and DMR 0231418). The authors are grateful to Dr. Clark Cooper, Dr. Jorn Larsen-Basse and Dr. Carmen Huber for their encouragement and support. Appreciation is extended to Prof. Marie Ange Arsène and to Prof. Jun Lou for useful discussions, and their help on the bridging models. The first author also expresses his gratitude to the National Council for Scientific and Technological Development (CNPq) and the Co-ordination for the Improvement of Higher Education Personnel (Capes) for their support, and to Mr. Leandro Cunha and Mr. Paulo Doniseti Silva for their skilful assistance at the Laboratory of Rural Construction of the Faculty of Animal Science and Food Engineering, University of São Paulo, Brazil.

References

[1] Swamy RN, editor. Natural fibre reinforced cement and concrete. Concrete technology and design, 5. Glasgow: Blackie; 1988.
[2] Savastano Jr H, Agopyan V, John VM. Low-cost roofing tiles based on vegetable fibre–cement composites. In: Proceedings of the CIB symposium on construction & environment. São Paulo: Escola Politécnica da Universidade de São Paulo/CIB; 2000. 10. p [CD-Rom].
[3] Coutts RSP. A review of Australian research into natural fibre cement composites. Cem Concr Compos 2005;27(5):518–26.
[4] Kung E, Mercer C, Allameh S, Popoola O, Soboyejo WO. An investigation of fracture and fatigue in a metal/polymer composite. Metall Mater Trans A 2001;32A(8):1997–2010.
[5] Lou J, Soboyejo WO. An investigation of the effects of loading rate on resistance-curve behavior and toughening in cast lamellar gamma-based titanium aluminides. Metall Mater Trans A 2001;32A(2):325–37.
[6] Savastano Jr H, Warden PG, Coutts RSP. Ground iron blast furnace slag as a matrix for cellulose-cement materials. Cem Concr Compos 2001;23(4–5):389–97.
[7] Savastano Jr H, Warden PG, Coutts RSP. Performance of low-cost vegetable fibre–cement composites under weathering. In: Duncan J, editor. Proceedings of the CIB World Building Congress. Branz: Wellington; 2001. p. 11 [CD-Rom].
[8] Savastano Jr H, Warden PG, Coutts RSP. Potential of alternative fibre cements as building materials for developing areas. Cem Concr Compos 2003;25(6):585–92.
[9] Savastano Jr H, Warden PG, Coutts RSP. Microstructure and mechanical properties of waste fibre–cement composites. Cem Concr Compos 2005;27(5):583–92.
[10] Higgins HG. Paper physics in Australia. Melbourne: CSIRO Division of Forestry and Forest Products; 1996.
[11] Savastano Jr H, Turner A, Mercer C, Soboyejo WO. Mechanical behavior of cement based materials reinforced with sisal fibers. J Mater Sci 2006;41:6938–48.

[12] Gram H-E. Durability of natural fibres in concrete. In: Swamy RN, editor. Natural fibre reinforced cement and concrete. Concrete technology and design, 5. Glasgow: Blackie; 1988. p. 143–72.
[13] Savastano Jr H, Agopyan V. Transition zone studies of vegetable fibre–cement paste composites. Cem Concr Compos 1999;21(1):49–57.
[14] Tolêdo Filho RD, Scrivener K, England GL, Ghavami K. Durability of alkali-sensitive sisal and coconut fibres in cement mortar composites. Cem Concr Compos 2000;22(2):127–43.
[15] Bentur A, Akers SAS. The microstructure and aging of cellulose fibre reinforced cement composites cured in a normal environment. Int J Cem Compos Lightweight Concr 1989;11(2):99–109.
[16] Wang S-D, Pu X-C, Scrivener KL, Pratt PL. Alkali-activated slag cement and concrete: a review of properties and problems. Adv Cem Res 1995;7(27):93–102.
[17] Chan Y-W, Li VC. Effects on transition zone densification on fiber/cement paste bond strength improvement. Adv Cem Based Mater 1997;5(1):8–17.
[18] Castro J, Naaman AN. Cement mortar reinforced with natural fibers. ACI J 1981;78(1):69–78.
[19] Shah SP, Marikunte SS. Fiber-reinforced concrete. In: Proceedings of the Center for Advanced Cement-Based Materials, Faculty Enhancement Workshop. Evanston: Northwestern University/NSF/ACBM Center; 1993. p. 226–52 [chapter 8].
[20] Balaguru PN, Shah SP. Fiber-reinforced cement composites. NY: McGraw-Hill; 1992.
[21] Eissa A-B, Batson G. Model for predicting the fracture process zone and R-curve for high strength FRC. Cem Concr Compos 1996;18(2):125–33.
[22] Nelson PK, Li VC, Kamada T. Fracture toughness of microfiber reinforced cement composites. J Mater Civ Eng 2002;14(5):384–91.
[23] Coutts RSP. From forest to factory to fabrication. In: Swamy RN, editor. Proceedings of the fourth international symposium on fibre reinforced cement and concrete. London: E&FN Spon; 1992. p. 31–47 [Rilem Proceedings, 17].
[24] Soboyejo WO. Toughening mechanisms. In: Soboyejo WO, editor. Mechanical properties of engineered materials. NY: Marcel Dekker Publishers; 2002. p. 414–55 [chapter 13].
[25] Shah SP, Swartz SE, Ouyang C. Fracture mechanics of concrete: applications of fracture mechanics to concrete, rock, and other quasi-brittle materials. NY: John Wiley & Sons; 1995.
[26] Coutts RSP. Sticks and stones...!! Forest Products Newsletter, 0816-1526 1986;2(1):1–8 [CSIRO Division of Chemical and Wood Technology, Australia].
[27] Oliveira CTA, John VM, Agopyan V. Pore water composition of activated granulated blast furnace slag. In: Proceedings of the second international conference on alkaline cements and concretes. Kiev: Kiev State Technical University of Construction and Architecture; 1999. p. 18–20.
[28] Associação Brasileira de Normas Técnicas. Cimento Portland de alto-forno, NBR 5735. Rio de Janeiro: ABNT; 1991. 5 p. [in Portuguese].
[29] Savastano Jr H, Warden PG, Coutts RSP. Brazilian waste fibres as reinforcement for cement-based composites. Cem Concr Compos 2000;22(5):379–84.
[30] Marikunte S, Soroushian P. Statistical evaluation of long-term durability characteristics of cellulose fiber reinforced cement composites. ACI Mater J 1994;91(6):607–16.
[31] Coutts RSP, Ridikas V. Refined wood fibre–cement products. Appita 1982;35(5):395–400.
[32] Bichard W, Scudamore P. An evaluation of the comparative performance of the Kajaani FS-100 and FS-200 fiber length analyzers. Tappi J 1988;71(12): 149–55.
[33] Appita. Kappa number of pulp, P201 m-86. Carlton: Appita; 1986. 4 p.
[34] Australian Standards. Freeness of pulp, AS 1301 206s-88. Sydney: Australian Standards; 1988. 9 p.
[35] Eusebio DA, Cabangon RJ, Warden PG, Coutts RSP. The Manufacture of wood fibre reinforced cement composites from *Eucalyptus pellita* and *Acacia mangium* chemi-thermomechanical pulp. In: Proceedings of the fourth Pacific Rim bio-based composites symposium. Bogor: Bogor Agricultural University; 1998. p. 428–36.
[36] Soboyejo WO, Venkateswara Rao KT, Sastry SML, Ritchie RO. Strength, fracture, and fatigue behavior of advanced high-temperature intermetallics reinforced with ductile phases. Metall Trans A 1993;24A(3):585–600.
[37] American Society for Testing and Materials. Standard test method for plane-strain fracture toughness of metallic materials, E399-90. West Conshohocken: ASTM; 1997. p. 31 [Book of Standards v. 03.01].
[38] Budiansky B, Amazigo JC, Evans AG. Small-scale crack bridging and the fracture-toughness of particulate-reinforced ceramics. J Mech Phys Solids 1988;36(2):167–87.
[39] Li M, Soboyejo WO. An investigation of the effects of ductile-layer thickness on the fracture behavior of nickel aluminide microlaminates. Metall Mater Trans A 2000;31A(5):1385–99.
[40] Bloyer DR, Rao KTV, Ritchie RO. Fracture toughness and R-curve behavior of laminated brittle-matrix composites. Metall Mater Trans A 1998;29A(10): 2483–96.
[41] Bloyer DR, Rao KTV, Ritchie RO. Fatigue-crack propagation behavior of ductile/brittle laminated composites. Metall Mater Trans A 1999;30A(3): 633–42.
[42] Fett T, Munz D. Stress intensity factors and weight functions for one-dimensional cracks. Institut fur Materialforschung, Kernforschungszentrum Karlsruhe; 1994 [Report KfK 5290].
[43] Bentur A. Fiber-reinforced cementitious materials. In: Skalny JP, editor. Materials science of concrete. Waterville: American Ceramic Society; 1989. p. 223–84.
[44] Banthia N, Sheng J. Fracture toughness of micro-fiber reinforced cement composites. Cem Concr Compos 1996;18(4):251–69.
[45] Beaudoin JJ. Handbook of fiber-reinforced concrete: principles, properties, developments and applications. Park Ridge: Noyes; 1990.
[46] Tolêdo Filho RD, Ghavami K, England GL, Scrivener K. Development of vegetable fibre–mortar composites of improved durability. Cem Concr Compos 2003;25(2):185–96.
[47] Pavasars I, Hagberg J, Borén H, Allard B. Alkaline degradation of cellulose: mechanisms and kinetics. J Polym Environ 2003;11(2):39–47.
[48] McMeeking RM, Evans AG. Matrix fatigue cracking in fiber composites. Mech Mater 1990;9(3):217–27.
[49] Ritchie RO. Mechanisms of fatigue-crack propagation in ductile and brittle solids. Int J Fract 1999;100:55–83.